Hindawi Publishing Corporation
Journal of Nanomaterials
Volume 2008, Article ID 352109, 7 pages
doi:10.1155/2008/352109

*Research Article*

# Atomic Force and Optical Microscopy Characterization of the Deformation of Individual Carbon Nanotubes and Nanofibers

**Terry P. Bigioni[1,2] and Brett A. Cruden[1]**

[1] *NASA Ames Research Center, University Affiliated Research Center (UARC), Moffett Field, California, CA 94035, USA*
[2] *Department of Chemistry, The University of Toledo, Toledo, OH 43606, USA*

Correspondence should be addressed to Brett A. Cruden, brett.a.cruden@nasa.gov

Received 4 September 2007; Revised 31 December 2007; Accepted 12 January 2008

Recommended by Jun Lou

A popular technique for characterizing the mechanical properties of carbon nanotubes is to apply a one-dimension axial compression and measure its response to the compressive force. At some critical compression, a dramatic decrease in the force is observed. This has previously been attributed to Euler buckling, allowing the elastic modulus to be calculated from the Euler buckling force. We have attached individual plasma enhanced chemical vapor deposition (PECVD) grown carbon nanofibers (CNFs) and thermal chemical vapor deposition (CVD) grown carbon nanotubes (CNTs) to the apex of an atomic force microscope (AFM) cantilever to examine this mechanical response. By combining the force measurements and simultaneous video microscopy, we are able to observe the mechanical deformation and correlate points in the force curve with phenomena such as slipping and bending. Analysis of the mechanical response must therefore be interpreted in terms of bending and/or slipping of a tube compressed by an off-normal force.

Copyright © 2008 T. P. Bigioni and B. A. Cruden. This is an open access article distributed under the Creative Commons Attribution License, which permits unrestricted use, distribution, and reproduction in any medium, provided the original work is properly cited.

## 1. INTRODUCTION

Carbon nanotubes (CNTs) have recently generated intense interest due to a combination of remarkable electrical, thermal, and mechanical properties. The mechanical properties have generated interest for producing high-strength lightweight composite materials [1]. The mechanical properties are also relevant for operation of CNTs as resonators [2], electromechanical relays [3, 4], or atomic force microscope (AFM) probe tips [5, 6]. Other applications utilizing CNTs as interfacial materials, such as thermal interface [7], dry adhesive [8], or super-compressible films [9], rely on the mechanical deformation and stiction properties of the CNT within an array or mat of CNTs.

Varied attempts have been made to measure the moduli and strengths of carbon nanotubes via approaches such as natural and driven resonance measurements and bending deformation under AFM measurement. The modulus of CNTs is measured at around 1.2 TPa with some studies suggesting a reduction in modulus as diameter and structural defects increase [10, 11]. A variation on the carbon nanotube, often called a carbon nanofiber (CNF), which is grown by plasma enhanced chemical vapor deposition (PECVD), should show a significant reduction in modulus relative to the CNT due to its stacked cone graphene morphology [12]. Still the CNF is of interest as it may be grown as a free standing, vertically aligned cylindrical nanostructure. While the data available on the mechanical properties of the CNF is fairly limited, they are still of interest for applications such as thermal interface materials [7, 13], AFM tips [5], and cellular probes [14].

The mechanical deflection behavior of these nanostructures needs to be understood in much broader terms than the basic modulus measurement. Specifically, it is not well known what the mechanical behavior and deformation modes of CNTs and CNFs are at an interface under compression. The nanotubes may deform by buckling, or they may slip at the interface. Local defects on the CNTs and CNFs may lead to a kinking behavior. These different modes of deformation are important in understanding

performance of the material in applications such as thermal interface and dry adhesives, where the actual areal overlap of the CNT with its contacted surface is likely the determining factor for thermal conduction or adhesion strength. CNTs present at a high packing may act as a metamaterial, where the bending, buckling, or slip of one tube may influence the motion and contact of neighboring tubes. Finally, phenomena such as plastic deformation and work hardening have also been observed in CNT and CNF arrays which are presently not well characterized or understood [9, 15].

While single CNTs have been attached to AFM tips and measured under a compressive load [16, 17], misalignments of the CNT with respect to the substrate and imperfections in the tubes themselves, such as curvature and lattice defects, can lead to bending, slipping, and kinking during compression. Measurement of the force response curve alone is not sufficient, in general, to distinguish these different modes of compressive response. This has been accomplished previously by visualizing deformation modes of CNTs under tensile and compressive loads in a scanning electron microscope (SEM) [18, 19] or transmission electron microscope (TEM) [20, 21].

We have devised a technically simpler method wherein we observe the tube motion using optical video microscopy while simultaneously measuring its compressive behavior. Our approach requires no specialized equipment, making it accessible to many more laboratories and applicable to a wide range of materials. Additionally, the approach can provide insight into how these systems behave under ambient conditions, rather than under vacuum. Although optical imaging provides only a two-dimensional projection of a three-dimensional geometry, and with limited spatial resolution, it serves as a qualitative guide for identifying events such as bending, kinking, and slipping for the purposes of interpreting force data. This allows for correlation of force response curves with the actual compressive responses of individual CNTs and CNFs.

## 2. EXPERIMENTAL

Carbon nanotubes were grown by thermal chemical vapor deposition on NiCr substrates as described in [22]. Carbon nanofibers were produced by PECVD in acetylene ammonia mixtures as described in [23]. The CNTs and CNFs were then attached to Ni-coated AFM tips as described in [24], as shown in Figure 2. In the case of the CNF, it was found that a side attachment of the CNF to the pyramid did not result in a strong attachment, and the CNF could be removed from the pyramid under repeated cycling. To address this issue, the CNF was brought into contact solely at the tip of the AFM pyramid, as shown in Figure 2(a). This resulted in a strong attachment of the CNF to the AFM tip. We believe this approach was effective because it increased the contact resistance between the CNF and AFM tip, producing sufficient contact heating to spot weld the CNF to the AFM tip. This process was not required in the case of the CNT due to a smaller cross-sectional area of the contact and/or a lower-electrical resistance for the CNT itself resulting in heat dissipation primarily at the contact rather than being divided between the contact and the interior of the CNT. The insets in Figures 2(a) and 2(c) highlight the differences in the attachment techniques for CNTs and CNFs.

Measurements were made on a Molecular Imaging Pico, scanning probe microscope operating in tapping mode. For the purposes of the measurement, the head was moved at a constant rate while monitoring the change in resonance amplitude as the tip moved in and out of contact with a Si wafer. It should be noted that the driving frequency was held constant near the free-resonance frequency of the cantilever throughout the experiment, such that the changing response is attributable to a combination of damping and resonance shift. A CCD camera coupled with a long working distance lens was used to image the motion of the AFM tip and attached CNT/CNF at a magnification of 500×. Images were $208 \times 160$ pixels and were captured at a frame rate of 20 fps. A customized sample plate holder was designed with a notch to accommodate the positioning of the objective lens. The scanner was also lowered to provide adequate clearance for the objective below the AFM body. A red filter was required to remove scattered laser light from the optical image. A fiber optic light source was positioned at each side of the AFM head to provide oblique illumination for dark-field imaging. The experimental set up is shown in Figure 1. The CCD camera output was sent to a computer for data storage and analysis.

The CNTs/CNFs were repeatedly cycled through compressions and generally reproduced each cycle, often in detail. These experiments were preferred for analysis. Occasionally, a tip-fiber weld would fail, as confirmed later by SEM, and the measurements would drastically change for subsequent cycles (not shown). It was possible to correlate video microscopy data with the AFM scanning by identifying sudden movements of the AFM cantilever that were coincident with scan start and stop commands from the AFM software. Logger Pro Software was employed to track motion of images collected.

It is well known that CNTs can be visualized in an optical microscope [25]. This is the predominant method used to attach CNTs to AFM tips as first demonstrated by Dai et al. [26]. While their paper claimed to visualize bundles, it has later been realized that individual tubes are also viewable this way [27]. An optical microscope cannot resolve the diameter of the CNT because it is smaller than the diffraction limit. The CNT can scatter light, however, and so can be routinely visualized in the dark field. This is analogous to visualizing individual metal nanoparticles by imaging the light scattered by their plasmon modes under darkfield illumination [28]. Namely, the diameter of the nanoparticles cannot be determined optically, but light scattered from single nanoparticles can be measured if they are isolated on a substrate. In contrast, the length of the CNT is several microns and is therefore well within the resolution limits of optical microscopy. In our system, the optical imaging corresponds to approximately 100 nm per pixel, therefore the deflections of the CNTs and CNFs under compression are also easily detected.

(a) (b)

Figure 1: Images of the setup. The long-working-distance microscopic lens is pointed at the AFM cantilever.

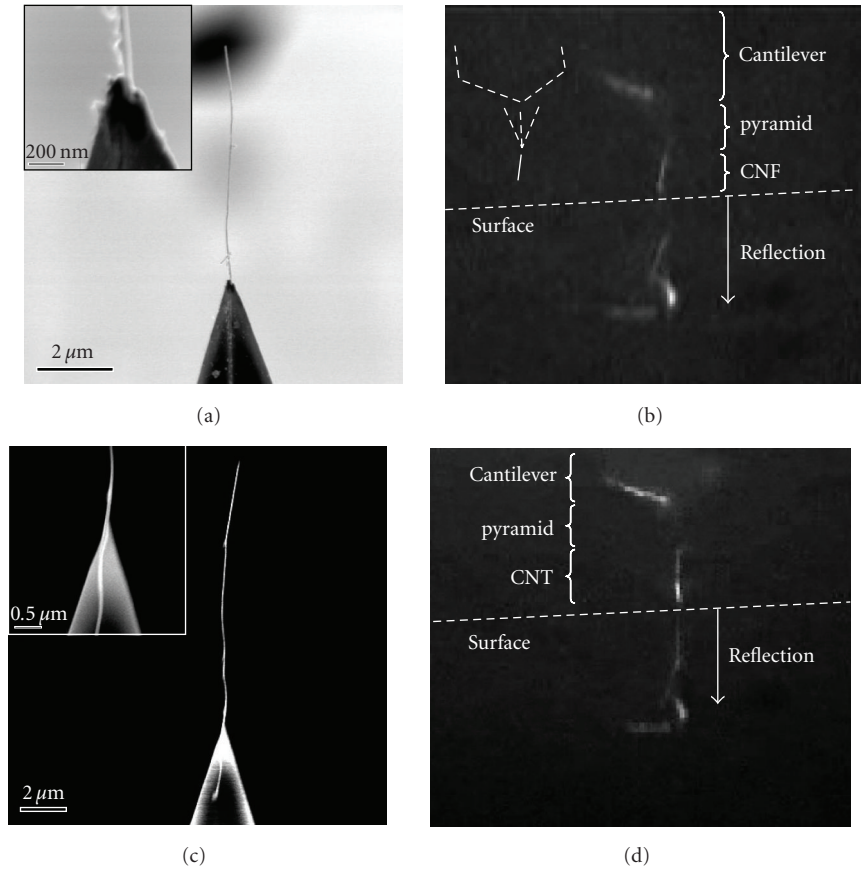


(a) (b)

(c) (d)

Figure 2: (a), (c) SEM and (b), (d) optical microscopy images of the AFM tips with attached nanostructures. Insets show close-up of the attachment points. Parts of the video image are labeled for clarity. The dashed lines in (b) show the profile of the cantilever, only part of which scatters light into the optical microscope. (a), (b) are for the carbon nanofiber and (c), (d) are for the carbon nanotube.

## 3. RESULTS AND DISCUSSION

Two representative data sets for CNT- and CNF-based deflection measurements will be discussed to illustrate the application of the technique. It should be noted that the difference between these measurements is not indicative of a difference between CNTs and CNFs per se, but is instead meant to illustrate different deformation modes observed through this approach. Further analysis and quantification would be required to gain a full understanding of the behaviors of CNTs and CNFs under compression, but this is beyond the scope of the current letter. Figure 2 shows SEM images of the CNT and CNF as attached to the AFM cantilever, along with the complimentary video capture images. The CNT is approximately 12 $\mu$m long while the CNF is approximately 6.5 $\mu$m long. This was sufficient for imaging under video capture (approximately 50–100 pixels per tube). Actual videos of the deflection during measurement are available as supplementary material online.

We must note that each mounted CNT and CNF has its own shape and structural defects and approaches the substrate at a different angle. Since dark-field imaging relies on

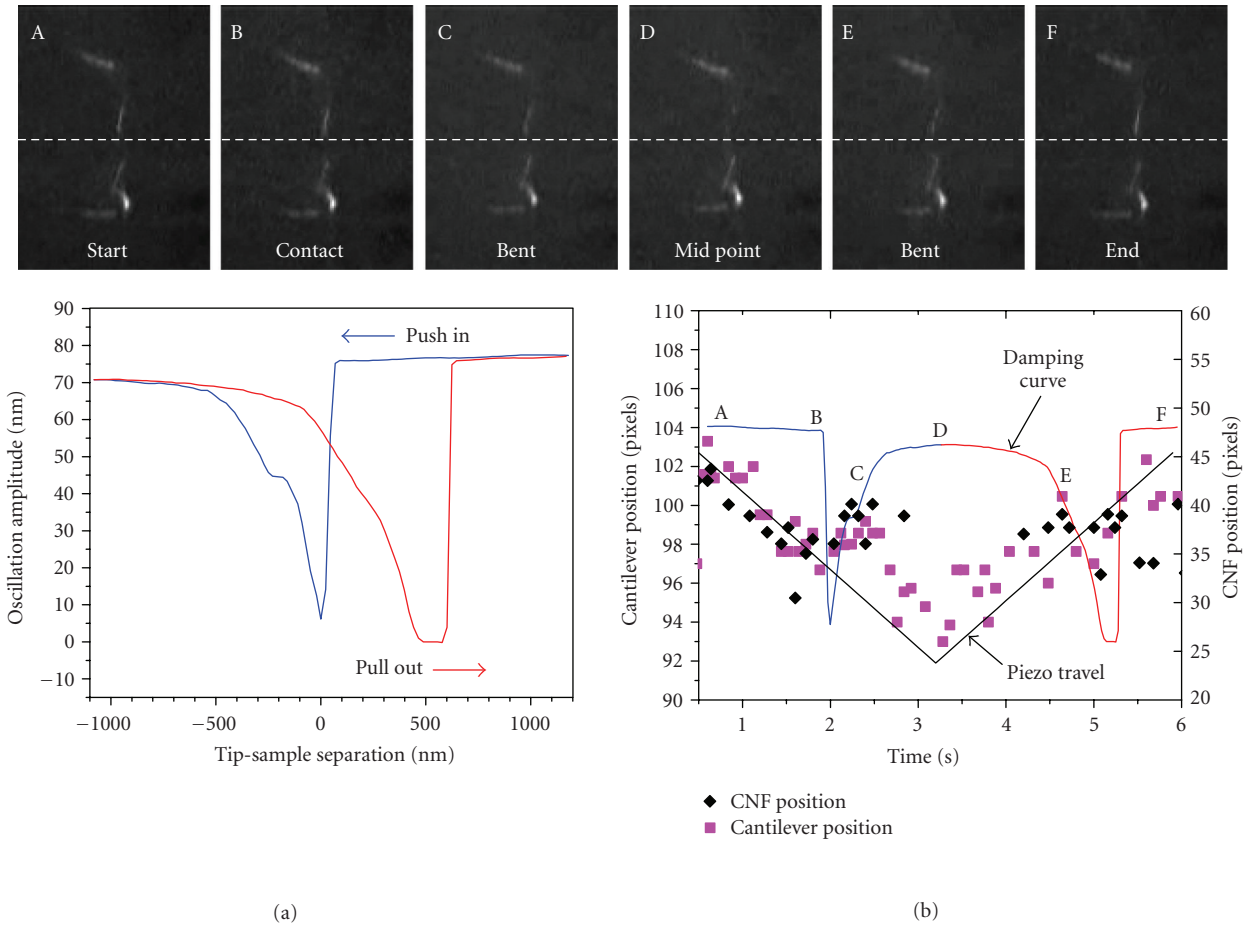


Figure 3: (a) Trace from the tapping mode AFM data for a carbon nanofiber tip, showing oscillation damping as tip sample separation is varied. (b) The same trace as a function of time, showing the AFM data and piezo travel. Several major points on the curve are labeled and the corresponding stills from the video are shown at these points. Also shown are points tracked during video capture, including cantilever position and position of the carbon nanofiber.

oblique light being scattered into the objective, each CNT and CNF looks different. The ability to identify bending, slipping, and kinking naturally differed for different experiments. In general, however, our observations indicate certain consistent optical behaviors, namely, (i) bending results in a slow change in illumination, (ii) slipping a discontinuous change, and (iii) kinking a slow change in one part of the tube and little in the other. Often a sharp bend is also observed for kinks. Similar observations are made during withdrawal, but occasionally the tube/fiber will appear to straighten and scatter more light than usual. This is likely due to tension, although it is difficult to distinguish exactly when contact is broken due to the short length scales and the imaging mode. These three different modes are demonstrated in supplemental video S1.

Figure 3, together with corresponding supplemental video S2, displays the response of the CNF under compression of up to 1.1 $\mu$m. Figure 3(a) shows the displacement-damping curve with corresponding video capture images from various points in the displacement cycle. Figure 3(b) shows $y$-axis pixel locations for tracking two prominent points in the video data—the end of the AFM cantilever and the upper end of the CNF. At initial contact, the CNF tip still appears fairly straight in the video microscopy and the AFM oscillation is immediately damped as the CNF is pressed into the surface. Under further depression, the system stiffness is reduced and oscillation amplitude begins to increase. This increase is accompanied by an apparent upward motion of both the cantilever and CNF tip. In this stage, deflection of the CNF is barely perceptible and the force is apparently being absorbed primarily by the cantilever. A brief plateau in the displacement-damping curve corresponds to the maximum deflection of the cantilever as load is transferred to the CNF. Following this plateau, a more visible bending of the CNF is apparent and the upward trend of displacement reverses. The cantilever displacement then follows the trend of the piezo displacement, while the separation between the CNF tip and piezo/cantilever decreases, corresponding to bending or buckling of the CNF.

At around 500 nm of compression, the CNF shape is distorted such that it is no longer trackable in the video, indicating that it is bent in such a way as to no longer scatter light

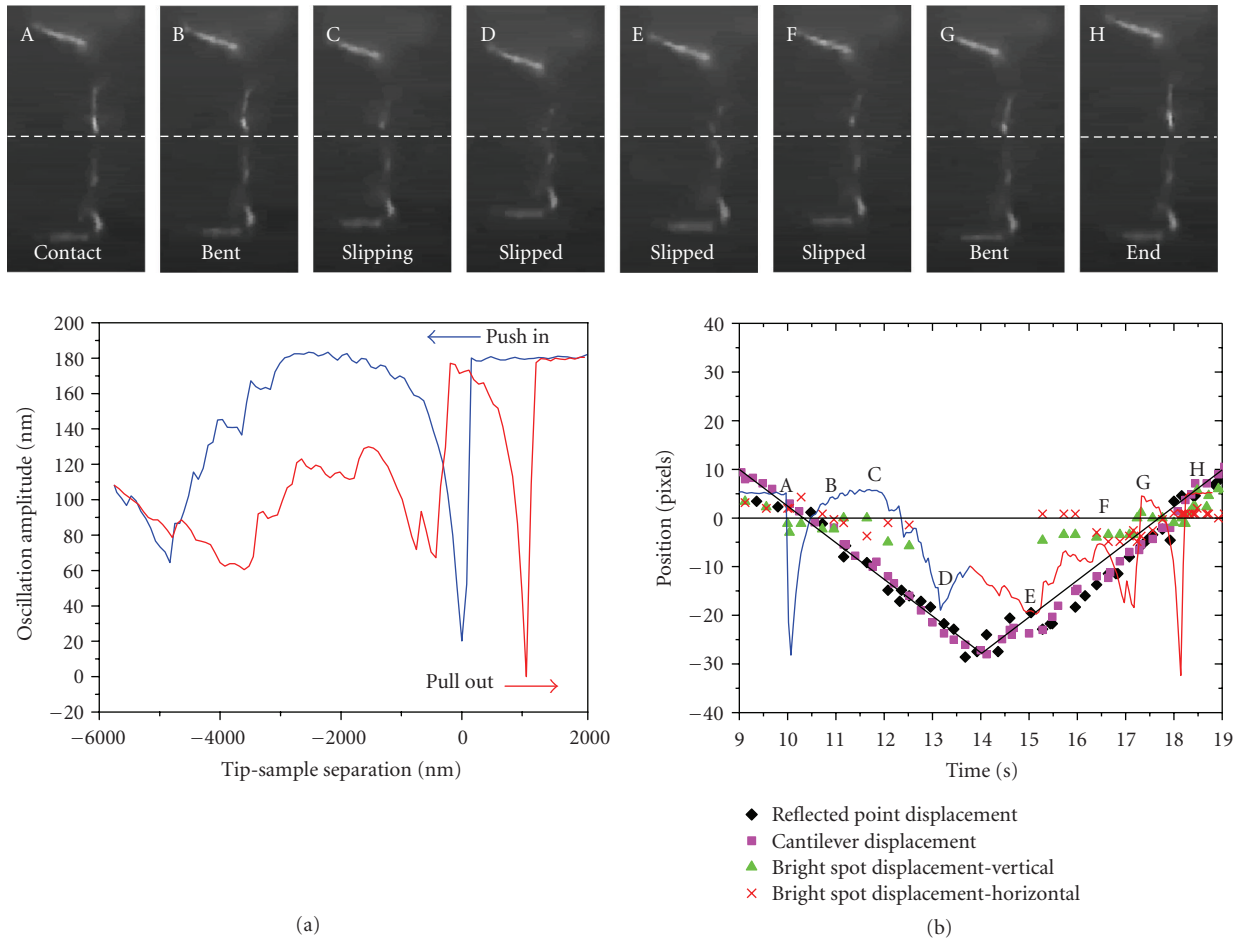


FIGURE 4: The same measurement as for Figure 3 for a carbon nanotube attached tip at higher degrees of compression. The points in (b) include motion tracked on the cantilever, the reflection of the cantilever, and horizontal and vertical displacements of the carbon nanotube.

into the objective. During this stage, the oscillation amplitude has reached a constant value close to the free oscillation amplitude. This indicates that the CNF is presenting a very low stiffness, consistent with a strongly bowed fiber. On pull-out, the CNF becomes visible again and the oscillation amplitude begins to decrease. Very little bending is observable on pull out—the CNF appears to be straight when the piezo displacement returns to zero, even though the oscillation amplitude is still decreasing. This hysteresis observed between scanning probe push-in and pull-out is often attributed to the properties of a water bridge formed between the tip and the substrate [29]. In this case, the water bridge provides an adhesion force and therefore tension on the CNF once the tip passes the initial contact point during withdrawal. The CNF may straighten under tension and reposition on the surface such that the contact angle approaches 90 degrees and the tip-substrate separation is maximized while still in contact. This could provide additional travel beyond the initial contact point, after which the water bridge collapses and separation is achieved.

Figure 4, together with supplemental video S3, shows similar data to Figure 3 for the CNTs under higher compression. The initial trends of the CNTs are nearly identical to that of the CNF. As the unbent CNT first makes contact with the surface the oscillation amplitude is immediately damped. As opposed to the previous case, no plateau in the damping curve or cantilever deflection is observed. This is attributed primarily to the curvature of the CNT reducing its resistance to buckling relative to the straighter CNF. The greater length of the CNT will reduce its stiffness by almost 8×, though this is expected to be compensated by a higher modulus in the CNT relative to the CNF. Further pushing of the tube results in buckling and a corresponding reduction in stiffness until, at 2 $\mu$m of compression, the oscillation amplitude has returned to nearly the free-oscillation amplitude and the CNT is clearly bowed. Further pushing leads to slip of the tube along the surface, and the CNT is no longer visible in the images. This results in a stiffening of the CNT as it slides along the surface in a stick-slip mode, leading to several ridges in the damping curve. Outside of the first slip event, this stick-slip action is inferred rather than observed directly because the CNT is not visible. Pull-out shows a similar series of ridges as the CNT unsticks and slides, eventually returning to a single point contact near the original cantilever position. Close inspection of Figure 4(b) shows that during pull-out these ridges are reflected in the motion of the cantilever

relative to the piezo line, which is not observed during push-in. At the point of zero tip-sample separation, the damping characteristics are determined by the water bridge and the cantilever is pulled approximately 1 $\mu$m further away than the initial contact separation when the water bridge collapses.

## 4. CONCLUSIONS

We have shown that it is possible to track motions of CNFs and CNTs with optical video microscopy during mechanical measurements of CNFs and CNTs that were mounted to AFM tips. Motions of the CNF/Ts and cantilevers in the optical images can be correlated with features in AFM measurements. Reductions in stiffness were correlated with bending modes and increases in stiffness can be attributed to slipping on the Si substrate. These measurements demonstrate that optical characterization of the mechanical response of nanotubes and fibers can aid in the interpretation of mechanical measurements, such as those demonstrated with AFM. Performing contact-mode AFM force measurements coupled with an inverted optical microscope that is equipped with dark-field optics should improve the quality of the data and may provide some unique insights into the mechanics of nanoscale objects.

## ACKNOWLEDGMENTS

The authors would like to thank Drs. Cattien Nguyen, Joseph Leung, and Alan Cassell for helpful discussions. Funding for the project was provided by the University of California Discovery Grant Program.

## REFERENCES

[1] O. Breuer and U. Sundararaj, "Big returns from small fibers: a review of polymer/carbon nanotube composites," *Polymer Composites*, vol. 25, no. 6, pp. 630–645, 2004.

[2] J. F. Davis, M. Bronikowski, D. Choi, et al., "High-Q mechanical resonator arrays based on carbon nanotubes," in *Proceedings of the 3rd IEEE Conference on Nanotechnology (NANO '03)*, vol. 2, pp. 635–638, San Francisco, Calif, USA, August 2003.

[3] S. W. Lee, D. S. Lee, R. E. Morjan, et al., "A three-terminal carbon nanorelay," *Nano Letters*, vol. 4, no. 10, pp. 2027–2030, 2004.

[4] B. A. Cruden and A. M. Cassell, "Vertically oriented carbon nanofiber based nanoelectromechanical switch," *IEEE Transactions on Nanotechnology*, vol. 5, no. 4, pp. 350–355, 2006.

[5] Q. Ye, A. M. Cassell, H. Liu, K.-J. Chao, J. Han, and M. Meyyappan, "Large-scale fabrication of carbon nanotube probe tips for atomic force microscopy critical dimension imaging applications," *Nano Letters*, vol. 4, no. 7, pp. 1301–1308, 2004.

[6] C. V. Nguyen, K.-J. Chao, R. M. D. Stevens, et al., "Carbon nanotube tip probes: stability and lateral resolution in scanning probe microscopy and application to surface science in semiconductors," *Nanotechnology*, vol. 12, no. 3, pp. 363–367, 2001.

[7] Q. Ngo, B. A. Cruden, A. M. Cassell, et al., "Thermal interface properties of Cu-filled vertically aligned carbon nanofiber arrays," *Nano Letters*, vol. 4, no. 12, pp. 2403–2407, 2004.

[8] Y. Zhao, T. Tong, L. Delzeit, A. Kashani, M. Meyyappan, and A. Majumdar, "Interfacial energy and strength of multiwalled-carbon-nanotube-based dry adhesive," *Journal of Vacuum Science and Technology B*, vol. 24, no. 1, pp. 331–335, 2006.

[9] A. Cao, P. L. Dickrell, W. G. Sawyer, M. N. Ghasemi-Nejhad, and P. M. Ajayan, "Materials science: super-compressible foamlike carbon nanotube films," *Science*, vol. 310, no. 5752, pp. 1307–1310, 2005.

[10] E. W. Wong, P. E. Sheehan, and C. M. Lieber, "Nanobeam mechanics: elasticity, strength, and toughness of nanorods and nanotubes," *Science*, vol. 277, no. 5334, pp. 1971–1975, 1997.

[11] Z. L. Wang, P. Poncharal, and W. A. de Heer, "Nanomeasurements of individual carbon nanotubes by *in situ* TEM," *Pure and Applied Chemistry*, vol. 72, no. 1-2, pp. 209–219, 2000.

[12] A. V. Melechko, V. I. Merkulov, T. E. McKnight, et al., "Vertically aligned carbon nanofibers and related structures: controlled synthesis and directed assembly," *Journal of Applied Physics*, vol. 97, no. 4, Article ID 041301, 39 pages, 2005.

[13] J. Xu and T. S. Fisher, "Enhancement of thermal interface materials with carbon nanotube arrays," *International Journal of Heat and Mass Transfer*, vol. 49, no. 9-10, pp. 1658–1666, 2006.

[14] T. D. B. Nguyen-Vu, H. Chen, A. M. Cassell, R. Andrews, M. Meyyappan, and J. Li, "Vertically aligned carbon nanoflber arrays: an advance toward electrical-neural interfaces," *Small*, vol. 2, no. 1, pp. 89–94, 2006.

[15] Y. Zhang, E. Suhir, and Y. Xu, "Effective Young's modulus of carbon nanofiber array," *Journal of Materials Research*, vol. 21, no. 11, pp. 2948–2954, 2006.

[16] S. I. Lee, S. W. Howell, A. Raman, R. Reifenberger, C. V. Nguyen, and M. Meyyappan, "Nonlinear tapping dynamics of multi-walled carbon nanotube tipped atomic force microcantilevers," *Nanotechnology*, vol. 15, no. 5, pp. 416–421, 2004.

[17] H. W. Yap, R. S. Lakes, and R. W. Carpick, "Mechanical instabilities of individual multiwalled carbon nanotubes under cyclic axial compression," *Nano Letters*, vol. 7, no. 5, pp. 1149–1154, 2007.

[18] W. Ding, L. Calabri, K. M. Kohlhaas, X. Chen, D. A. Dikin, and R. S. Ruoff, "Modulus, fracture strength, and brittle vs. plastic response of the outer shell of arc-grown multi-walled carbon nanotubes," *Experimental Mechanics*, vol. 47, no. 1, pp. 25–36, 2007.

[19] M. F. Yu, M. J. Dyer, G. D. Skidmore, et al., "Three-dimen sional manipulation of carbon nanotubes under a scanning electron microscope," *Nanotechnology*, vol. 10, no. 3, pp. 244–252, 1999.

[20] T. Kuzumaki and Y. Mitsuda, "Nanoscale mechanics of carbon nanotube evaluated by nanoprobe manipulation in transmission electron microscope," *Japanese Journal of Applied Physics, Part 1*, vol. 45, no. 1, pp. 364–368, 2006.

[21] M. Nakajima, F. Arai, and T. Fukuda, " *In situ* measurement of Young's modulus of carbon nanotubes inside a TEM through a hybrid nanorobotic manipulation system," *IEEE Transactions on Nanotechnology*, vol. 5, no. 3, pp. 243–248, 2006.

[22] B. Ribaya, J. Leung, M. Rahman, and C. V. Nguyen, "A study on the mechanical and electrical reliability of individual carbon nanotube field emission cathodes," to appear in *Nanotechnology*.

[23] B. A. Cruden, A. M. Cassell, Q. Ye, and M. Meyyappan, "Reactor design considerations in the hot filament/direct current plasma synthesis of carbon nanofibers," *Journal of Applied Physics*, vol. 94, no. 6, pp. 4070–4078, 2003.

[24] C. V. Nguyen, R. M. D. Stevens, J. Barber, et al., "Carbon nanotube scanning probe for profiling of deep-ultraviolet and 193 nm photoresist patterns," *Applied Physics Letters*, vol. 81, no. 5, pp. 901–903, 2002.

[25] J. Gaillard, M. Skove, and A. M. Rao, "Mechanical properties of chemical vapor deposition-grown multiwalled carbon nanotubes," *Applied Physics Letters*, vol. 86, no. 23, Article ID 233109, 3 pages, 2005.
[26] H. Dai, J. H. Hafner, A. G. Rinzler, D. T. Colbert, and R. E. Smalley, "Nanotubes as nanoprobes in scanning probe microscopy," *Nature*, vol. 384, no. 6605, pp. 147–150, 1996.
[27] C. V. Nguyen, Q. Ye, and M. Meyyappan, "Carbon nanotube tips for scanning probe microscopy: fabrication and high aspect ratio nanometrology," *Measurement Science and Technology*, vol. 16, no. 11, pp. 2138–2146, 2005.
[28] J. J. Mock, D. R. Smith, and S. Schultz, "Local refractive index dependence of plasmon resonance spectra from individual nanoparticles," *Nano Letters*, vol. 3, no. 4, pp. 485–491, 2003.
[29] J. Jang, M. Yang, and G. Schatz, "Microscopic origin of the humidity dependence of the adhesion force in atomic force microscopy," *Journal of Chemical Physics*, vol. 126, no. 17, Article ID 174705, 6 pages, 2007.

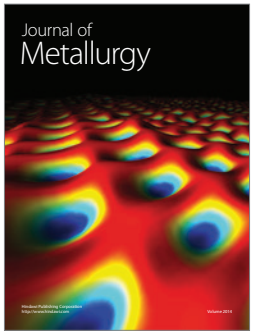

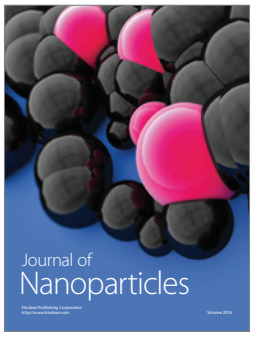

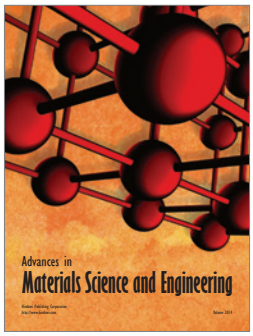

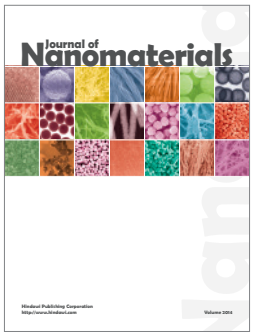

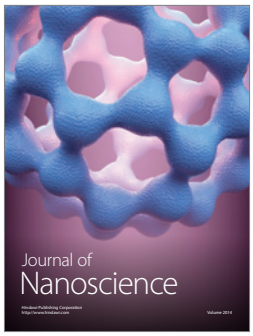

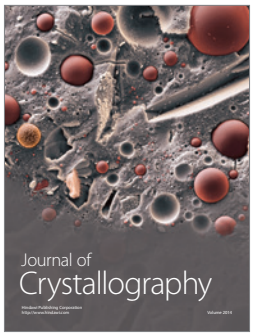


Hindawi

Submit your manuscripts at
http://www.hindawi.com